Determining Metallicities of RR Lyrae Variables from Photometric Light Curves through Period-ϕ_{31}-Metallicity Relationship

A Dissertation Report Submitted in Partial Fulfilment

of the Requirements for the Degree of

Master in Science

by

Mahiguhappriyaprakash*

Supervised by Prof. Harinder P. Singh

Submitted on May 25, 2024

Department of Physics and Astrophysics,

University of Delhi,

Delhi - 110007

Session 2023-2024

*Examination Roll Number: 22222762128, Email: manjulaprakash2002@gmail.com

Abstract

This dissertation reports the establishment of a new, calibrated relationship between pulsation period, Fourier parameter ϕ_{31}, and metallicity (Fe/H) for RR Lyrae stars in the visible region. RR Lyrae stars are pulsating variable stars crucial for distance determination and galactic structure studies. An accurate period-ϕ_{31}-Fe/H relation is vital for these purposes.

This work presents the newly calibrated relation derived from Gaia DR3[1] photometric data of 83 out of 108 stars that were taken from Gilligan et al. (2021) The derived relation is then compared with existing relationships established in prior literature studies. A detailed analysis is provided to assess the viability and potential improvements offered by the newly calibrated relation.

The key findings of the dissertation are expected to include:

- The specific form and coefficients of the established period-ϕ_{31}-Fe/H relation.
- A comparison of our relation with existing literature, highlighting any agreements or discrepancies.

This dissertation aims to contribute valuable insights into the pulsation properties and metallicity dependence of RR Lyrae stars, ultimately improving our understanding of stellar populations and galactic evolution.

[1] Gaia Collaboration et al. (2023)

DECLARATION

This dissertation report is submitted in partial fulfilment of the requirements for the degree of Master of Science (Physics) and was conducted under the supervision of Prof. Harinder P. Singh. I declare that this report is my own work and contains no plagiarism. There has been no submission of the work to any other institute for a degree or certificate. In drafting the dissertation, I followed the requirements supplied by the institution. I have provided proper credit to other sources wherever I have used resources (data, theoretical analysis, figures, and text) from them by citing them in the dissertation text and providing their details in the references.

MAHIGUHAPPRIYAPRAKASH

Place: Delhi

Date: 27/05/2024

CERTIFICATE

This is to certify that **Mahiguhappriyaprakash**, bearing Examination Roll Number **22222762128**, has prepared this dissertation entitled "Determining Metallicities of RR Lyrae Variables from Photometric Light Curves through Period-ϕ_{31}-Metallicity Relationship", under my supervision in partial fulfilment of the requirements for the degree of Master of Science (M.Sc.) in Physics at the Department of Physics and Astrophysics, University of Delhi, Delhi-110007, India.

Prof. Harinder P. Singh

(Thesis Advisor)

Place: Delhi

Date: 27.5.2024

Acknowledgements

Completing this thesis has been a journey enriched by the support of many. My deepest gratitude goes to my supervisor, Prof. Harinder P. Singh, whose guidance, expertise, and encouragement were instrumental in shaping this work. I am also grateful to my senior colleague Mr. Nitesh Kumar, for sharing their knowledge in analysis of photometric data and for their constant support. To my parents, Mrs. Manjula S. and Mr. Prakash D., thank you for your unwavering love, constant encouragement, and unwavering support that made this possible. Finally, to my friends and all those who offered patience, understanding, and encouragement during difficult times, my sincere thanks. This thesis is a testament to the collective support of all these wonderful people.

MAHIGUHAPPRIYAPRAKASH

Table of Contents

List of Figures

List of Tables

Main Content

1 Introduction

Variable stars are those stars whose luminosity varies periodically over time. The variability depends on two factors: *intrinsic and extrinsic*. Intrinsic variability is due to the physical changes inside the star, giving rise to pulsation and eruption, while extrinsic variability is due to external reasons like eclipses and stellar rotation. RR Lyrae are those variables that are identified with the horizontal branch part of the HR Diagram (Figure 1.1), where the pulsations are driven due to the instabilities in the He II convection zone, giving rise to changes in the opacity. They are one of the most used tracers for old stellar population in the Milky Way as well as for the Local Group galaxies. RRLs are of three types based on their mode of pulsation:

- RRab (fundamental mode),
- RRc (1^{st} overtone mode), and
- RRd (both fundamental and 1^{st} overtone mode)

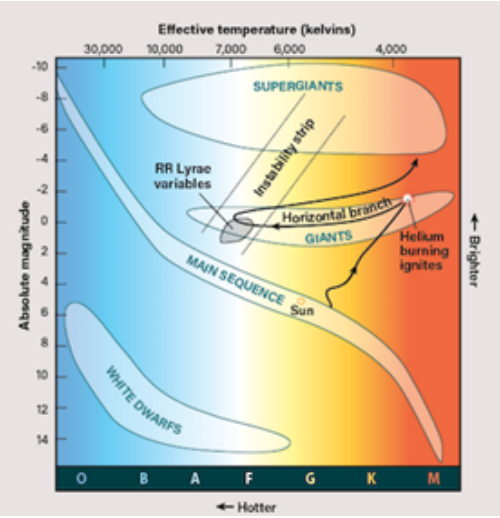

Figure 1.1: Location of RR Lyrae in the Hertsprung-Russell diagram. Source: Astronomy Magazine (July 2020 pp 59)

RRab's have longer period, larger amplitudes and sawtooth-like light curves (Figure 1.2), while RRc's have comparatively shorter period. Kramer's rule is given as:

$$K \propto \frac{\rho}{T^{3.5}} \tag{1.1}$$

Here, K is the opacity, ρ is the density and T is the temperature of the region. As the ionization zone of singly and doubly ionized Helium compresses, density increases and extra energy goes into ionization, temperature being constant throughout. As a result, the opacity increases and the layers expand outwards. As they cool down, recombination can happen resulting in decrease in opacity. The layer collapses and restarts back. This gives rise to pulsation in these regions. Recent studies have revealed that they can be used as standard candles because of the existence of a definitive relationship between their period, luminosity, and metal abundances. However, the quest to find a method to determine the accurate metallicities in an efficient method is still on.

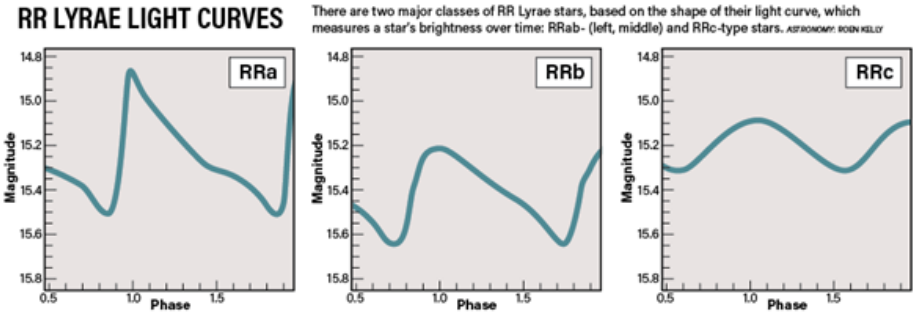

Figure 1.2: Light curves of different types of RR Lyrae. Source: Astronomy Magazine (July 2020 pp 59)

1.1 Spectroscopy in Astronomy

Traditionally, the determination of metal abundance in stellar sources require knowledge of their *spectra*. Acquiring a spectroscopic data requires a lot of work. There are three possible ways to use spectroscopic analysis in determining metallicity:

- ΔS method
- HRS

the most recent extension being, G-band Gaia DR2 and ASAS-SN V-band light curves. Our work primarily focuses on deriving a new period-ϕ_{31}-[Fe/H] relation in V-band for a set of galactic RRLs using photometric methods.

This report is structured as follows. In Section §2 we describe in detail about the photometric data of a set of stars that we had obtained from the Gaia database and how it has been calibrated to use further in our analysis. In Section §3, we go through the data analysis in great detail: Subsection §3.1 is all about the calibration of photometric light curves of the samples under analysis and Subsection §3.2 explains about the process of removal of galactic dust extinctions from our light curves. The following two parts - Subsection §3.3 and §3.4 - are the main part of our analysis. The former deals with the Fourier decomposition of light curves and the latter deals with the formulation of the empirical period-ϕ_{31}-metallicity([Fe/H]) relationship for the given set of RRLs. The discussions on our final relation and its comparison with other literature and the spectroscopic metallicity is given in Section §4 and our conclusions are presented in Section §5.

2 Data and Methodology

This work has made use of data from the European Space Agency (ESA) mission *Gaia*[2], processed by the *Gaia* Data Processing and Analysis Consortium (DPAC[3]). Funding for the DPAC has been provided by national institutions, in particular the institutions participating in the *Gaia* Multilateral Agreement. In this work we utilize the stars analysed by Gilligan et al. (2021)(hereafter CKG), which mainly focuses on stars present in the Chadid et al. (2017) sample. Out of the 108 stars presented in CKG's work, 89 stars (all of them being RRab) were chosen based on visual examination of the star's phased light curve. The photometric data of these stars were obtained from the Gaia DR3 database using the Gaia ID supplied in the supplementary material[4] of CKG. The V-band magnitudes were obtained by using Equation 2.1 that converts the G (white light) , G_{BP} (blue

[2] Prusti et al. (2016);https://www.cosmos.esa.int/gaia
[3] https://www.cosmos.esa.int/web/gaia/dpac/consortium
[4] https://shorturl.at/I7PXb

- Photometric metallicities through color and shape of light curves

The ΔS *method* utilizes the Medium Resolution Spectral (MRS) data and relies on ratios between the equivalent widths of Ca and H lines. One such application of this method are shown in Liu et al. (2020) which utilizes the LAMOST data and is based on a fit of theoretical models. This suggests that ΔS method is pretty reliable in determining the metal abundances with an uncertainty of 0.2-0.3 dex.

High Resolution Spectra(HRS) on the other hand provides direct measurement of metallicity with an uncertainty of 0.1 dex. While both ΔS method and HRS are equally reliable, they still require spectra. Obtaining the spectra of stars require large amount of telescope and analysis time. Also, these methods are not directly applicable to a large number of RRLs that are located in the Milky Way and other Local Group galaxies. Thus a reliable and precise method is necessary to probe into distances that cannot be reached by spectroscopy or at higher extinction environments.

In such cases, what we resort to is the *photometric metallicity*. As mentioned earlier, regions with higher extinction can only be probed photometrically by near-infrared telescopes like the James Webb Space Telescope (JWST).

1.2 Photometric Metallicities

Early work by Jurcsik and Kovacs (1996)(hereafter JK96) has demonstrated that the shape of the fundamental mode RRLs (RRab) at optical wavelengths is directly related to its metal abundance. Their work presents a linear relationship connecting the star's [Fe/H] with its period of pulsation and the lower order Fourier parameters (ϕ_{31}) obtained from the Fourier decomposition of its light curve in the V-band. This has been proven to give the most sensitive diagnostics about the star's metallicity. Further work by Nemec et al. (2013)(hereafter N13), Martinez-Vazquez et al. (2016), Smolec (2005), Ngeow et al. (2016), Iorio and Belokurov (2021)(IB20) and Mullen et al. (2021)(M21) extended this analysis, respectively, to well-sampled RRab light curves obtained from Kepler space telescope (Koch et al. (2010)) to include stars from globular clusters to various survey programs like the I-band Optical Gravitational Lensing Experiment, R-band Palomar Transient Factory and,

wavelength) and G_{RP} (red wavelength) magnitudes that were available in the raw data to V-band:

$$V = G - 0.02704 + 0.01424(G_{BP} - G_{RP}) - 0.2156(G_{BP} - G_{RP})^2 + 0.01426(G_{BP} - G_{RP})^3 \quad (2.1)$$

The python routine to perform this task is available on my *GitHub*[5] repository. Once the V-band magnitudes are obtained, we phase the raw light curves. For this, we need periods of the respective light curves. This information is extracted directly from the supplementary material where the periods are quoted as log(P). Then we proceed to the Fourier decomposition of the phased light curves, followed by the determination of the period-ϕ_{31}-[Fe/H] relation.

3 Analysis

Now that we have the magnitudes of the stars in V-band, we will proceed with the calibration of the light curves: obtaining a phased light curves from the raw Gaia light curves.

3.1 Calibration of Light Curves

As mentioned previously, the optical time series data of 89 galactic RRLs were obtained from Gaia DR3 survey. Figure 3.1 shows an example time series light curve of one of the samples under analysis. We require the knowledge of the period P of light curve to determine the phase. The period of each raw light curve is already available in the supplementary material of CKG (Table 3.1) which were taken from Mullen et al. (2021) and re-derived using the Lombe-Scargle method[6].

[5] https://github.com/luciferAT02/RRLs/blob/main/phase_magnitude.py

[6] A powerful technique used to detect periodic signals in unevenly sampled data. It is particularly useful in astronomy for analyzing the light curves of stars or other celestial objects that might not have been observed at perfectly regular intervals.

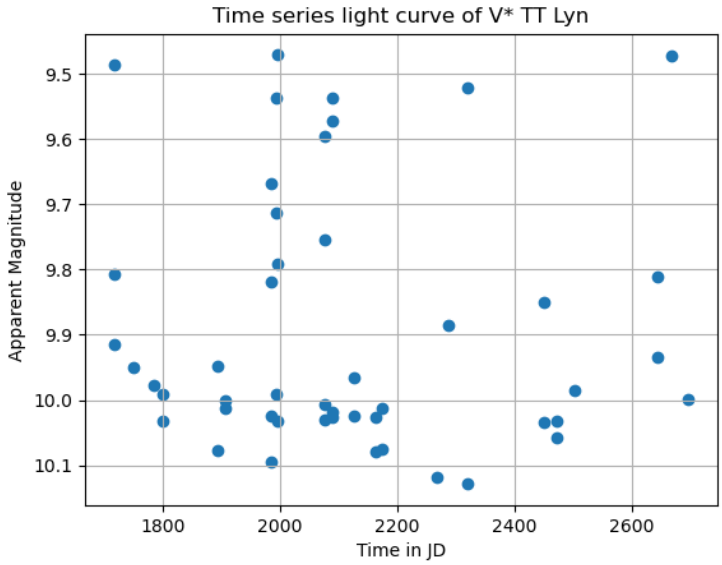

Figure 3.1: Time series light curve of V* TT Lyn in V-band obtained from Gaia DR3. The raw data consists of magnitudes only in G-, BP- and RP- bands. The conversion to V-band was done using Equation 2.1.

Gaia DR3 ID	m_V	m_V **Error**	**Period (logP)**	**Reddening**(A_V)	**[Fe/H]**	**[Fe/H] Error**
3111925220109675136	11.5276	0.0252	-0.322095	0.12	-0.6	0.13
5360400630327427072	11.3856	0.014	-0.277834	0.319	-1.6	0.13
3604450388616968576	11.4926	0.0096	-0.211066	0.14	-1.6	0.13
3677686044939929728	11.3491	0.0195	-0.279211	0.112	-2.2	0.13
5335614752064948224	11.9208	0.0222	-0.343723	0.567	-2.35	0.13
5810433728873201408	12.2945	0.0143	-0.326237	0.211	-0.75	0.13
5390917850431396224	12.0843	0.0176	-0.322593	0.177	-1.4	0.13
3030561879348972544	11.3091	0.0109	-0.134184	0.638	-1.4	0.13
6701724002113004928	11.9687	0.0111	-0.279842	0.44	-1.7	0.13
2371321782802181888	11.6571	0.0144	-0.231895	0.09	-1.45	0.13

Table 3.1: A sample table of the supplementary material of CKG. Note that the Fe/H values determined over here is via ΔS method.

To calculate the phase, we need an epoch reference time t_0. In a unevenly-spaced light curve like the one shown above, the time of first observation is not a great choice. So we choose the epoch

reference time to be the one at which the brightness is the maximum, that is, the magnitude is the minimum. Now, we use Equation 3.1 to determine the phase at each observation time to obtain the final phased light curve:

$$\Phi = \frac{(t - t_0)}{P} \tag{3.1}$$

where, t is the time of observation at each point. Figure 3.2 shows the phased light curve of V* TT Lyn. The python routine used to perform the above mentioned task is available on my *GitHub*[7] repository.

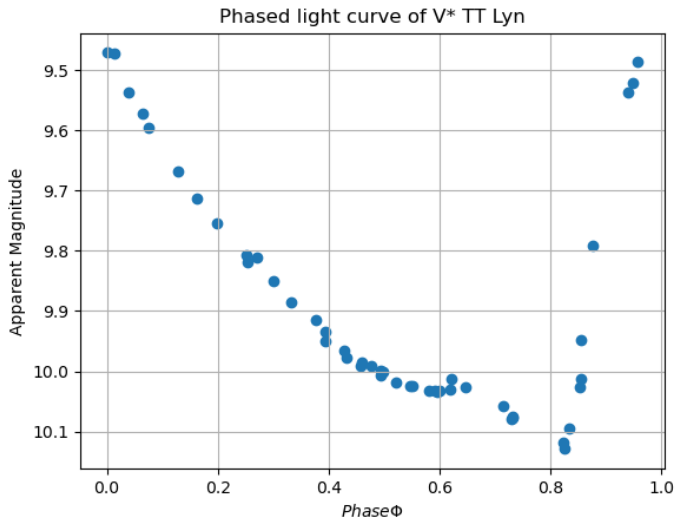

Figure 3.2: Phased light curve of V* TT Lyn obtained using the Python routine. Note that the light curve takes the sawtooth-shape.

3.2 Galactic Dust Extinctions

When we look at a star, the magnitude that we perceive is its apparent magnitude plus some external factors. These external factors are mainly due to the dust present in the earth's atmosphere and in the interstellar medium (ISM). Dust can scatter, absorb and polarize electromagnetic radiation. When the observer looks at a star through intervening dust, the effective dimming is caused by a combination of absorption and scattering. The collective effect of such factors are coined to be

[7] https://github.com/luciferAT02/RRLs/blob/main/phase_magnitude.py

extinction. Since different wavelengths of light are scattered and absorbed by the dust in different ways, extinction is a strong function of wavelength. Since our sample is a collection of galactic RRLs, it is required that we account for the extinction due to the galactic dust. The reddening by dust is expressed in terms of a *color excess* as:

$$E(B-V) = A_B - A_V \tag{3.2}$$

where $E(B-V)$ is the color excess, A_B and A_V are the extinctions in blue and visible wavelengths respectively (extinction at shorter wavelength minus extinction at longer wavelength). The ratio of total selective extinction is given as:

$$R_V = \frac{E(B-V)}{A_V} \tag{3.3}$$

The typical value of R_V chosen in astronomical literature is 3.1 for the lower-density portion of the ISM. Figure 3.3 shows the graph of R_V versus wavelength λ in different regions in and around the galaxy. For our samples we have used the web-based tool, *IRSA Dust Map Viewer*[8], for calculating the extinction in the V-band.

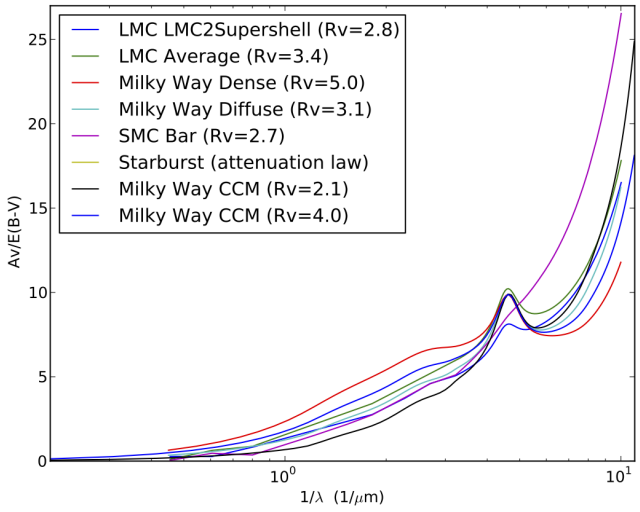

Figure 3.3: Extragalactic extinction curves taken from Calzetti et al. (2000)

[8] https://irsa.ipac.caltech.edu/applications/DUST/

Object Name	**RA**	**DEC**	$E(B-V)_{SandF}$	$\sigma_{E(B-V)_{SandF}}$	$A_V(SandF)$
V* AA CMi	109.32988	1.72779	0.0994	0.0029	0.3082
V* AF Vel	163.26037	-49.90632	0.2752	0.0068	0.8532
V* AM Vir	200.88888	-16.66608	0.0628	0.0015	0.1948
V* AT Vir	193.79392	-5.45898	0.0271	0.001	0.084
V* BI Cen	176.47758	-59.3779	0.7289	0.0316	2.2596
V* EX Aps	267.9375	-69.33471	0.0722	0.0018	0.2239
V* HK Pup	116.195	-13.09898	0.3087	0.0109	0.9569
V* MS Ara	270.76788	-52.72238	0.1063	0.0017	0.3296
V* RU Cet	15.16792	-15.95767	0.0207	0.0006	0.0642
V* RX Eri	72.43454	-15.74118	0.0572	0.0018	0.1773

Table 3.2: This table consists of the color excess and the dust extinction in V band calculated with reference to Schlafly and Finkbeiner (2011)(SandF) for the first 10 stars in our sample. The complete table is available in Appendix A.

Table 3.2 shows us the color excess and dust extinction in V band obtained from the IRSA dust extinction tool. The python routine to query Simbad for the names of the stars and making a IRSA-readable table is available in my GitHub[9] repository. We subtract $A_V(SandF)$ from the V-band magnitude calculated using Equation 2.1 before doing the Fourier decomposition of our phased light curves.

3.3 Fourier Decomposition

To find the metallicity of the star, we are required to study in detail about the shape of its phased light curve. Fourier decomposition is a widely used tool to quantify the shape of a light curve. To fully characterize the shape of a light curve, one requires only the lower order terms in the Fourier expansion (Simon and Lee (1981), hereafter SL81). The Fourier expansion of the magnitude in

[9] https://github.com/luciferAT02/RRLs/blob/main/Extinctions.ipynb

terms of the phase is given as:

$$m(\Phi) = A_0 + \sum_{n=1}^{n} A_i sin[2\pi i(\Phi + \Phi_0) + \phi_i] \tag{3.4}$$

where $m(\Phi)$ is the observed magnitude in V band, A_0 is the mean magnitude, n is the order of expansion, Φ is the phase obtained from the phased light curve varying from 0 to 1 and Φ_0 corresponds to the phase at time of maximum light t_0. A_i and ϕ_i are the i-th order Fourier amplitude and phase coefficients, respectively.

We determine the Fourier parameters by locally fitting Equation 3.4 to the phased light curve. We use the *curve_fit* routine of the SciPy[10] module, which uses the Levenberg-Marquardt (LM) algorithm, widely used in case of non-linear least square fit. The python routine used for the same is available on my *GitHub*[11] repository. We found out that a fourth order (n = 4) Fourier expansion was sufficient to reproduce the shape of the light curve. Any order greater than n = 4 would over-fit the curve. Figure 3.4 shows the Fourier-fitted phased light curve of a sample star.

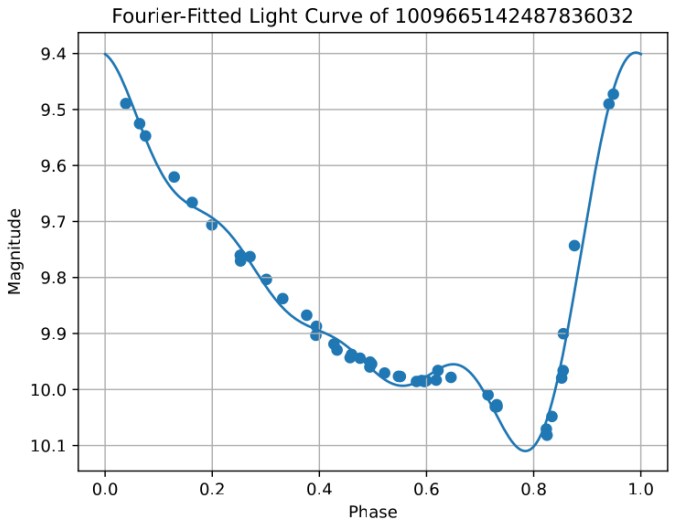

Figure 3.4: Fourier-fitted phased light curve of V* TT Lyn

[10] https://docs.scipy.org/doc/scipy/reference/generated/scipy.optimize.curve_fit.html
[11] https://github.com/luciferAT02/RRLs/blob/main/Fourier_Fit.py

Gaia ID	**Period**	m_0	A_1	A_3	ϕ_1	ϕ_3
3111925220109675136	0.476	11.245	0.325	0.072	3.634	4.117
5360400630327427072	0.527	10.567	0.328	0.090	3.883	4.102
3604450388616968576	0.615	11.321	0.239	0.067	3.783	4.349
3677686044939929728	0.526	11.293	0.415	0.146	4.156	4.143
5335614752064948224	0.453	9.684	0.368	0.140	3.862	3.654
5810433728873201408	0.472	12.121	0.398	0.133	3.863	4.341
3030561879348972544	0.734	10.355	0.251	0.060	4.224	6.050
6701724002113004928	0.525	11.707	0.321	0.079	4.179	5.057
2371321782802181888	0.586	11.611	0.341	0.090	4.112	4.814
2981136563934324224	0.587	9.520	0.299	0.104	4.002	4.816

Table 3.3: Table of Fourier coefficients evaluated by the python routine for the first 10 stars out of 89 stars in the sample. Full table available in Appendix B

Table 3.3 shows the Fourier parameters of first 10 stars generated using the python routine. SL81 first demonstrated that a certain combination of these Fourier parameters were directly related to some physical parameters of the pulsating star. These are defined either as a linear combination of the parameters (Equation 3.5) or the ratios of Fourier amplitudes (Equation 3.6).

$$\phi_{ij} = j.\phi_i - i.\phi_j \tag{3.5}$$

$$R_{ij} = \frac{A_i}{A_j} \tag{3.6}$$

Using the fact from SL81 and JK96 that the plot between ϕ_{31} and period showing a more pronounced separation between stars with different metallicities and a tighter correlation with less scatter in the data, suggesting a more precise relation, we use ϕ_{31} for our analysis. The uncertainties in the ϕ_{31} calculations are much smaller than the uncertainties in our metallicity measurements, a few stars whose error in ϕ_31 was greater than our chosen threshold (0.2). Such stars were removed from the calibration, leaving only 83 stars for the final calibration. Figure 3.5 shows the plot of ϕ_{31} versus the period of the 83 stars under consideration. Due to the 2π periodic ambiguity in the ϕ_31 coefficient,

some ϕ_{31} values required adding 2π to their phase in order to lie closer to the mean ϕ_{31} value, as suggested by JK96.

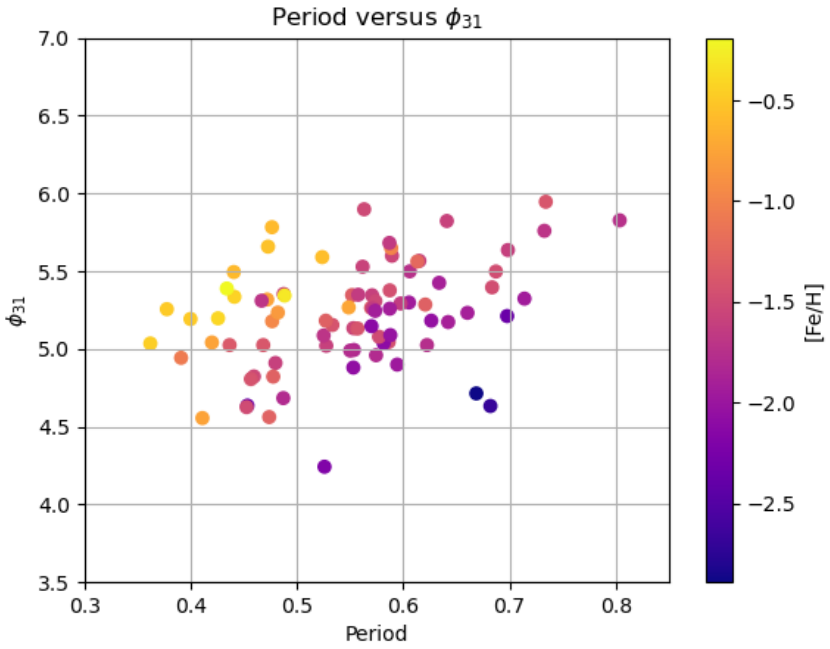

Figure 3.5: Fourier parameter ϕ_{31} versus period of the 83 sample stars that are color-coded according to their spectroscopic [Fe/H] values. The range goes as metal-rich in the top (yellow) to metal-poor in the bottom (dark-purple).

3.4 Period-ϕ_{31}-[Fe/H] fitting

We now have the required quantities in order to obtain a general relation between [Fe/H], period and ϕ_{31}:

- The calibrated [Fe/H] obtained by ΔS method in CKG,
- The period of each star in the sample obtained using Lombe-Scargle method in CKG, and
- The Fourier parameter ϕ_{31} which would give us the inherent information about the metallicity of the star from its light curve, that is, the photometric metalllicity.

To put them all together, we have fitted a linear relation between [Fe/H], period and ϕ_{31} as shown in Equation 3.7. We adopted Orthogonal Distance Regression (ODR) routine part of the SciPy[12] for multiple-variable linear regression. This method utilizes a modified trust-region Levenberg-Marquardt-type algorithm (Boggs and Rogers (1990)) to estimate the best fitting parameters. The primary reason to choose ODR for fitting is because it minimizes the perpendicular distance to the fit with no differentiation between dependent and independent variables. This is necessary because metallicity here is estimated indirectly, and its measurements might have inherent uncertainties. Also, it minimizes the sum of the squared perpendicular distances between the data points and the fitted model. This approach considers both horizontal and vertical deviations, ensuring a good fit not only along the x-axis (period) but also along the y-axis (ϕ_{31}).

$$[Fe/H] = a + b.(P - P_0) + c.(\phi_{31} - \phi_{31_0}) \tag{3.7}$$

Here P_0 and ϕ_{310} are pivot offsets necessary to add an extra element of robustness in the fitting procedure and reduce the fitting parameter uncertainties. Our best fit period-ϕ_{31}-Fe/H] relation based on the V-band light curves is:

$$[Fe/H] = (-1.46 \pm 0.04) + (-4.68 \pm 0.62).(P - 0.55) + (0.86 \pm 0.11).(\phi_{31} - 5.22) \tag{3.8}$$

The python routine used to fit the relation is available in my GitHub[13] repository.

4 Discussion

4.1 Comparison with spectroscopic metallicities

Although we have obtained our period-ϕ_{31}-[Fe/H] relation for our sample, it is essential to test if this provides consistent values of [Fe/H] for individual stars. To do this, we first predict [Fe/H] of individual stars using the obtained relation 3.8 and plot them against the [Fe/H] obtained using ΔS method by CKG. Figure 4.1 shows the same. Negative values of [Fe/H] suggests that the stars

[12] https://docs.scipy.org/doc/scipy/reference/odr.html
[13] https://github.com/luciferAT02/RRLs/blob/main/PLZ_relationship.ipynb

are metal-poor as compared to the Sun. The points are well within the RMS dispersion ($\sigma = 0.31$) and the errors in the calibrated [Fe/H] are within the RMS range. This suggests that the [Fe/H] obtained from Equation 3.8 correlates well with that of the [Fe/H] obtained from spectroscopic methods.

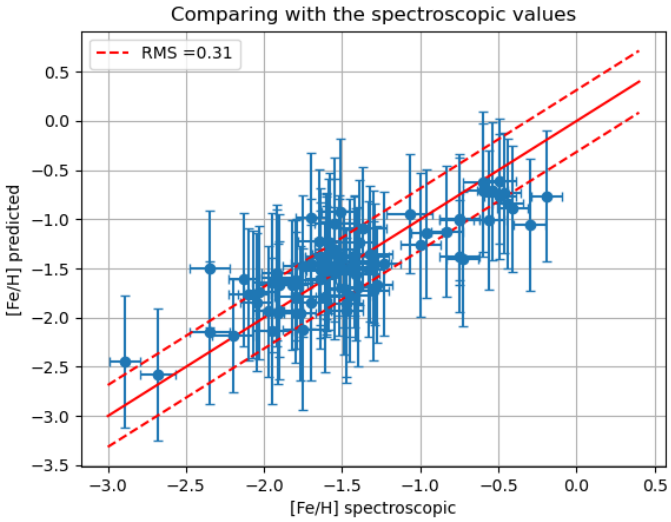

Figure 4.1: Spectroscopic [Fe/H] versus photometric [Fe/H] of the sample stars along with the error bars in both of the values.

Gaia ID	**Period**	ϕ_{31}	**[Fe/H]**	**[Fe/H] error**	**[Fe/H] predicted**	**[Fe/H] predicted (error)**
3111925220109675136	0.476	5.783	-0.6	0.13	-0.6223	0.7141
5360400630327427072	0.527	5.020	-1.6	0.13	-1.5191	0.6527
3604450388616968576	0.615	5.566	-1.6	0.13	-1.4587	0.7330
3677686044939929728	0.526	4.242	-2.2	0.13	-2.1824	0.5784
5335614752064948224	0.453	4.636	-2.35	0.13	-1.5033	0.5926
5810433728873201408	0.472	5.318	-0.75	0.13	-1.0023	0.6658
3030561879348972544	0.734	5.946	-1.4	0.13	-1.6887	0.8089
6701724002113004928	0.525	5.087	-1.7	0.13	-1.4507	0.6583
2371321782802181888	0.586	5.045	-1.45	0.13	-1.7736	0.6740
2981136563934324224	0.587	5.377	-1.45	0.13	-1.4920	0.7059

Table 4.1: This table contains the spectroscopic and photometric metallicities along with their errors respectively, for first 10 stars. Full table available in Appendix C

4.2 Comparison with other literature

In this section, we compare our optical period-ϕ_{31} -[Fe/H] relation (Equation 3.8) with previous relations found in the literature for similar wavelength ranges. In particular, we focus on the relations found in JK96, N13, IB20 and M21. The period-ϕ_{31}-[Fe/H] relation of JK96 reads as:

$$[Fe/H]_{JK96} = -5.038 - 5.394.Period + 1.345.\phi_{31}; \sigma = 0.38 \tag{4.1}$$

Their relation was derived using a total of 81 field RRab with V -band photometry from heterogeneous observations at various sites.

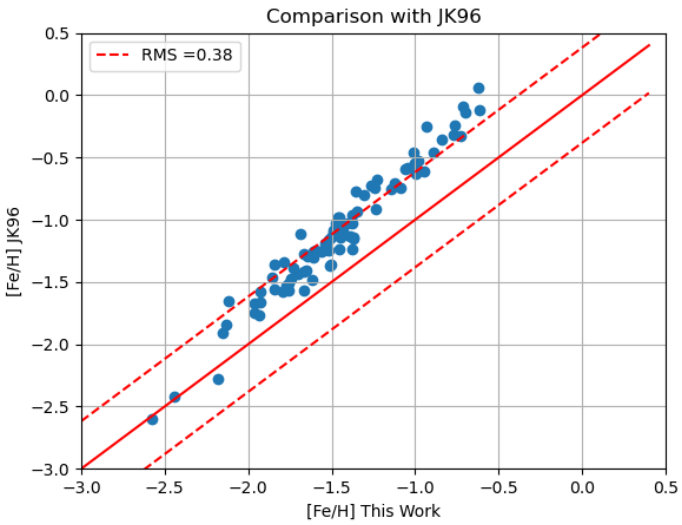

Figure 4.2: Comparison of our relation with that of JK96. The RMS dispersion comes out to be $\sigma = 0.38$. The red dashed lines around the 1:1 secant (solid line) represent the RMS dispersion between this work and the literature [Fe/H] abundance.

Figure 4.2 shows the comparison with the formula found in JK96(Equation 4.1). Their relation was derived using a total of 81 field RRab with V-band photometry from heterogeneous observations at various sites. Since JK96 adopted metallicities from high dispersion spectroscopy scale of Jurcsik (1995), for consistency we converted the metallicity derived by them to the scale in Carretta et al.

(2009), given by the formula in Kapakos et al. (2011):

$$[Fe/H]_{C09} = 1.001[Fe/H]_{JK96} - 0.112 \tag{4.2}$$

We found agreement with the relation found in JK96 to a large extent, with most of the stars lying within the RMS dispersion (red dashed lines) with $\sigma = 0.38$, which is much smaller than the uncertainty in the calculated [Fe/H].

N31 introduced a non-linear relation between period, ϕ_{31} and [Fe/H] which reads as:

$$[Fe/H] = b_0 + b_1.Period + b_2.\phi_{31} + b_3.Period.\phi_3 1 + b_4.\phi_{31}^2; \sigma = 0.6 \tag{4.3}$$

where $b_0 = -8.65$, $b_1 = -40.12$, $b_2 = 5.96$, $b_3 = 6.27$ and $b_4 = -0.72$. Their relation was calibrated using stars observed in the Kepler photometric band during the first 970 days of the Kepler mission. Due to Kepler's fixed field of view and shallow depth of the field, their calibration dataset had only 26 RRab stars, out of which 9 of them were Blazhko.[14]

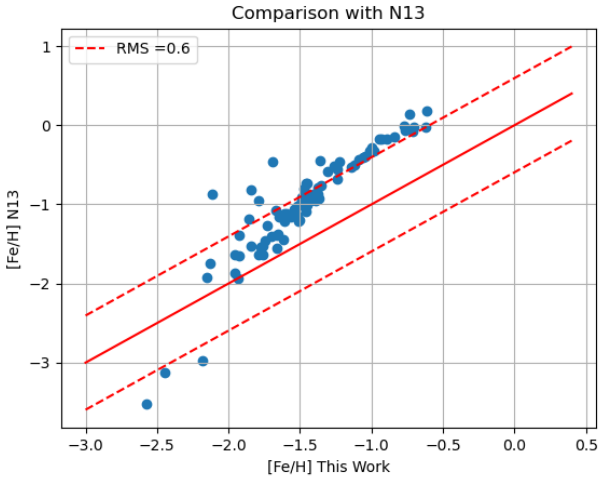

Figure 4.3: Comparison of our relation with that of N13. The RMS dispersion comes out to be $\sigma = 0.6$. The red dashed lines around the 1:1 secant (solid line) represent the RMS dispersion between this work and the literature [Fe/H] abundance.

[14]RRLs with periodic, or nearly periodic, long term modulation in their light curve.

In order to use the relation given by N13 with our relation, the V-band ϕ_{31} must be converted to that of Kepler band. This was done using Equation 4.4 derived by Nemec et al. (2011):

$$\phi_{31}(V) = \phi_{31}(Kp) - (0.151 \pm 0.026) \tag{4.4}$$

Figure 4.3 shows the comparison of our relation with that of N13. This relation was already calibrated in the C09 scale, so re-scaling is not required. From the graph, we can see that our relation matches really well with N13 in the higher metallicity region. There is a huge deviation in the low metallicity region, caused by the non-linear terms in Equation 4.3.

IB20 introduced a G-band period-ϕ_{31}-[Fe/H] relationship for RRab stars which were calibrated using a sample of 84 stars based on Gaia DR2 light curves. The relation is given in Equation 4.5

$$[Fe/H]_{IB20} = -1.68 - 5.08.(Period - 0.6) + 0.68.(\phi_{31} - 2.0); \sigma = 0.2 \tag{4.5}$$

Since this relation was determined in G-band system, it is necessary to convert our V-band ϕ_{31} to that of G-band using the relation given by Clementini et al. (2016):

$$\phi_{31}(G) = (0.104 \pm 0.020) + (1.000 \pm 0.008)\phi_{31}(V) \tag{4.6}$$

To set the coefficients on the same scale as that of IB20 , an additional offset of π is subtracted from ϕ_{31}. Metallicity in IB20 were on the scale of Zinn and West (1984)(ZW84) and thus were converted using the following relation given by IB20 :

$$[Fe/H]_{C09} = 1.105[Fe/H]_{ZW84} + 0.160 \tag{4.7}$$

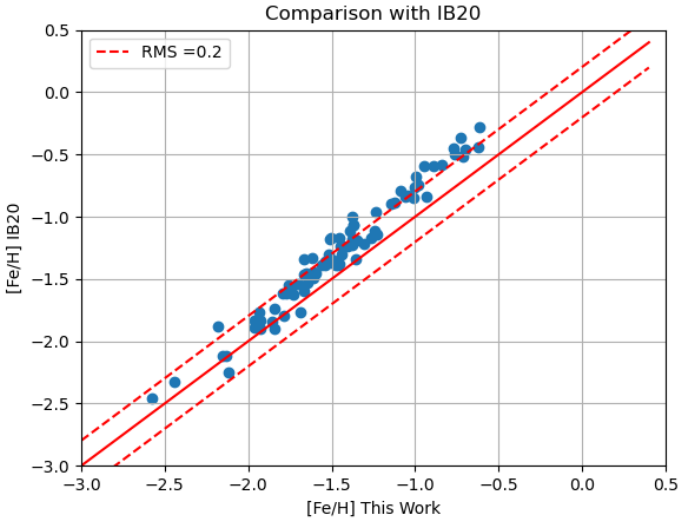

Figure 4.4: Comparison of our relation with that of IB20 . The RMS dispersion comes out to be $\sigma = 0.2$. The red dashed lines around the 1:1 secant (solid line) represent the RMS dispersion between this work and the literature [Fe/H] abundance.

From Figure 4.4 we can see that our relation matches quite well with that of IB20 , as compared to that of JK96 or N13. The RMS dispersion is also the lowest, ($\sigma = 0.2$) showing a good correlation. This could be because of the shared light curve source (Gaia) which ensures a consistent quality of ϕ_{31} values.

Lastly, we will compare the relation given by M21 which focuses on the stars in the HR+ΔS metallicity catalog that have a match in the ASAS-SN survey and have used 1980 RRLs with well-sampled light curves. Their period-ϕ_{31}-[Fe/H] relation reads as:

$$[Fe/H]_{M21} = -1.22 - 7.60.(Period - 0.58) + 1.42.(\phi_{31} - 5.25); \sigma = 0.56 \tag{4.8}$$

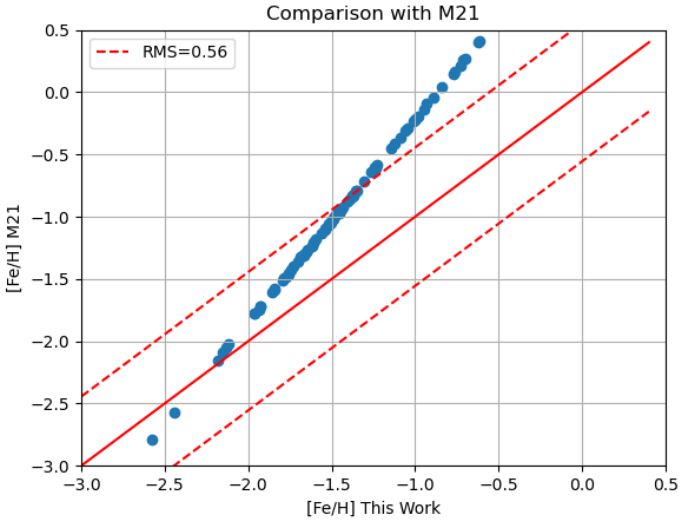

Figure 4.5: Comparison of our relation with that of M21. The RMS dispersion comes out to be $\sigma = 0.56$. The red dashed lines around the 1:1 secant (solid line) represent the RMS dispersion between this work and the literature [Fe/H] abundance.

A scale offset of 0.08 was then added to transform the C09 scale to that adopted by M21 HR+ΔS calibration sample. Figure 4.5 shows that there is a good correlation between our relation and that of M21 in the lower metallicity region. Also, there is a huge deviation in the trend at higher metallicity region. This suggests that our relation agrees well with that of M21 only at lower metallicity range.

5 Conclusions

This study established a new period-ϕ_{31}-[Fe/H] relation (Equation 3.8) for determining the metallicity of RR Lyrae stars using optical photometry. We have comprehensively compared this relation with existing literature to assess its validity and performance across various wavelength bands and metallicity ranges. Here are the key findings from our analysis:

- Our relation demonstrates good correlation with the established spectroscopic method (ΔS method by CKG), confirming its ability to provide reliable metallicity estimates (Figure 4.1).
- The relation shows good agreement with JK96(V-band) and IB20 (G-band), with RMS dispersions of $\sigma = 0.38$ and $\sigma = 0.2$, respectively (Figures 4.2, 4.4). This suggests the effectiveness of our relation for these bands, (potentially due to similar data sources (Gaia) and consistent ϕ_{31} quality in case of IB20).
- N13 (Kepler-band) exhibits a good match in the higher metallicity region but deviates at lower metallicities (Figure 4.3). This can be attributed to the non-linear terms present in N13's relation. V-band to Kepler-band conversion using Equation 4.4 was necessary for the comparison.
- M21 (based on HR+ΔS calibration) agrees better with our relation in the lower metallicity regime (Figure 4.5). This suggests our relation might be more suitable for stars with lower metallicities within that specific calibration sample. A scale offset was required to account for the difference between C09 and HR+ΔS metallicity scales.

This study offers a valuable addition to the existing methods for determining metallicity in RR Lyrae stars using optical photometry. Our relation provides a reliable alternative, particularly when using V-band or G-band data, due to the good agreement with JK96 and IB20 relations.

Appendices

A Dust Extinction Table

Object Name	**RA**	**DEC**	$E(B-V)_{SandF}$	**stdev**$E(B-V)_{SandF}$	$A_V(SandF)$
V* RY Col	78.78242	-41.62824	0.0251	0.0011	0.0779
V* ST Vir	216.91279	-0.90161	0.0359	0.0005	0.1114
V* SW For	45.28625	-38.12868	0.0129	0.0006	0.0401
V* SX For	52.59313	-36.05375	0.012	0.0009	0.0372
CD-38 1780	73.31004	-37.82109	0.0123	0.0007	0.0382
V* U Lep	74.07496	-21.21723	0.0294	0.0015	0.091
V* U Pic	72.52763	-50.65701	0.0084	0.0002	0.0261
V* UU Cet	1.02133	-16.99765	0.0196	0.0006	0.0606
V* V413 CrA	281.99008	-37.73959	0.0881	0.0033	0.273
V* V674 Cen	210.85029	-36.40561	0.0744	0.0013	0.2306
V* VW Dor	91.9405	-66.97746	0.0559	0.0013	0.1733
V* VY Ser	232.75804	1.68382	0.036	0.0004	0.1116
V* WY Ant	154.02063	-29.72845	0.0584	0.0009	0.1811
V* WY Pav	269.0515	-57.16206	0.093	0.0009	0.2882
V* X Crt	177.23425	-10.44126	0.0241	0.0011	0.0748
V* Z Mic	319.09458	-30.28419	0.0829	0.0028	0.2571
V* SU Col	76.946	-33.86513	0.0199	0.0004	0.0618
V* AR Per	64.32167	47.40018	1.1234	0.0241	3.4826
V* DR And	16.29462	34.21841	0.033	0.001	0.1022
V* CI And	28.78454	43.76569	0.0578	0.0019	0.1793
V* RR Leo	151.93108	23.99176	0.0373	0.0035	0.1155
V* TT Lyn	135.78246	44.58559	0.0153	0.0005	0.0475

V* SU Dra	174.48588	67.32974	0.0085	0.0004	0.0265
V* RS Boo	218.38838	31.75461	0.0127	0.0009	0.0394
V* ST Boo	232.66346	35.78453	0.0171	0.0002	0.0531
V* W CVn	211.61658	37.82818	0.0038	0.0005	0.0119
V* UZ CVn	187.61542	40.5089	0.0204	0.0011	0.0631
V* RV UMa	203.32533	53.98739	0.0167	0.001	0.0519
V* SW Dra	184.44429	69.51062	0.0125	0.0001	0.0388
V* DX Del	311.86817	12.46408	0.1163	0.0018	0.3604
V* NR Lyr	287.11346	38.81281	0.1476	0.0078	0.4577
V* KX Lyr	278.31342	40.17299	0.0581	0.004	0.18
V* XZ Cyg	293.12213	56.38819	0.1096	0.0024	0.3399
V* XZ Dra	287.42754	64.85893	0.0659	0.0016	0.2041
V* RX Cet	8.4095	-15.48744	0.0246	0.0007	0.0763
V* DN Aqr	349.82167	-24.21634	0.022	0.0007	0.0683
V* BR Aqr	354.63704	-9.31874	0.0238	0.0003	0.0739
V* BK Eri	42.48271	-1.42003	0.0469	0.0017	0.1454
V* RR Cet	23.03404	1.34173	0.0203	0.0003	0.0628
V* SW Aqr	318.82438	0.07635	0.0744	0.004	0.2307
V* BH Peg	343.25433	15.78795	0.0721	0.0008	0.2234
V* AS Vir	193.19113	-10.26011	0.0352	0.0009	0.109
V* SS Leo	173.47704	-0.03334	0.0174	0.0004	0.054
V* AA Aql	309.56283	-2.89028	0.0717	0.0059	0.2223
V* IO Lyr	275.65833	32.95906	0.0576	0.0039	0.1785
V* TW Her	268.63	30.41047	0.0373	0.0012	0.1156
V* W Tuc	14.54042	-63.39566	0.0179	0.0002	0.0554
V* HH Pup	110.14817	-46.70836	0.152	0.0054	0.4713
V* RV Oct	206.63225	-84.40177	0.1518	0.0104	0.4705

V* XZ Aps	223.02258	-79.6796	0.1267	0.0063	0.3928
V* BK Tuc	352.38883	-72.54439	0.0232	0.0004	0.072
V* V Ind	317.87458	-45.07455	0.0425	0.0009	0.1318
V* V1645 Sgr	305.18533	-41.11827	0.0541	0.0016	0.1676
V* V440 Sgr	293.08658	-23.85354	0.0833	0.002	0.2583
V* SZ Hya	138.45338	-9.3191	0.0319	0.0008	0.099
V* XX Lib	226.79179	-25.99764	0.1257	0.0125	0.3897
V* V2178 Cyg	295.02904	38.97232	0.188	0.0066	0.5828
V* V808 Cyg	296.41263	39.51486	0.2004	0.0074	0.6213
V* V782 Cyg	297.82083	40.44589	0.4455	0.0208	1.381
V* V783 Cyg	298.21975	40.79319	0.378	0.0126	1.1717
V* V784 Cyg	299.09542	41.33984	0.3017	0.0086	0.9353
ATO J295.3333+46.3912	295.33333	46.39129	0.1361	0.0052	0.4219
ASAS J192325+4231.7	290.85221	42.52844	0.0928	0.005	0.2876
V* V368 Lyr	287.7225	43.41527	0.0523	0.0024	0.1621
ASAS J185038+4125.4	282.65721	41.4238	0.0899	0.0055	0.2786
V* V354 Lyr	283.20983	41.56371	0.0859	0.0026	0.2663
V* V355 Lyr	283.35796	43.15456	0.071	0.004	0.2201
V* NQ Lyr	286.95158	42.29853	0.0573	0.0025	0.1777
V* V360 Lyr	285.49433	46.44601	0.0428	0.0009	0.1325
V* V350 Lyr	282.28483	46.19859	0.0439	0.0009	0.1361
V* V2470 Cyg	289.9915	46.88925	0.0585	0.0012	0.1813
V* V839 Cyg	290.07871	47.13014	0.0611	0.0015	0.1895
ATO J294.5798+46.4630	294.57983	46.46303	0.1283	0.0032	0.3978
V* V366 Lyr	287.41933	46.28834	0.055	0.0017	0.1706

ROTSE1 J190058.77+484441.5	285.24492	48.74509	0.0468	0.0021	0.1452
V* AW Dra	285.2	50.09199	0.0406	0.0008	0.1258
V* V1104 Cyg	289.50204	50.75495	0.072	0.0016	0.2231
V* CD Vel	146.15937	-45.87698	0.2578	0.0055	0.7993
V* TY Gru	334.16425	-39.93832	0.0129	0.0006	0.0399
BPS CS 22881-0039	332.39762	-40.43088	0.0123	0.0002	0.0381

Table A.1: This table consists of the color excess and the dust extinction in V band calculated with reference to Schlafly and Finkbeiner (2011)(SandF) for the stars other than those mentioned in 3.2.

B Fourier Parameters Table

Gaia ID	**Period**	m_0	A_1	A_3	ϕ_1	ϕ_3
4818854972838127360	0.479	10.861	0.341	0.068	4.239	5.154
3652665558338018048	0.411	11.472	0.487	0.155	4.067	4.189
5045760843864182528	0.804	12.265	0.232	0.055	4.145	5.695
4860671839583430912	0.605	11.064	0.239	0.066	3.915	4.478
4818348922610995200	0.420	12.174	0.412	0.128	4.243	5.205
2973463347160718976	0.581	10.563	0.389	0.116	4.180	5.009
4784552718312266624	0.440	11.437	0.328	0.097	3.868	4.533
2414817603803476864	0.606	11.984	0.224	0.068	3.977	4.863
6730211038418525056	0.589	10.303	0.228	0.057	4.175	5.557
6120897123486850944	0.494	11.110	0.333	0.102	3.832	4.881
5283957629860435072	0.571	11.617	0.361	0.100	3.798	4.172
4417888542753226112	0.714	9.986	0.235	0.043	4.162	5.242
5461994302138361728	0.574	10.687	0.297	0.109	3.996	4.381

5918501428232052992	0.589	11.828	0.242	0.072	3.664	4.075
3587566361077304704	0.733	11.362	0.230	0.066	3.826	4.671
6787617919184986496	0.587	11.343	0.240	0.069	4.480	0.272
4825302302864705152	0.487	12.528	0.317	0.097	4.151	5.239
234108363683247616	0.426	6.987	0.325	0.102	3.979	4.569
315028326379733760	0.563	12.375	0.374	0.091	3.949	5.177
349612816093349120	0.485	12.038	0.269	0.059	3.676	3.970
630421935431871232	0.452	10.673	0.425	0.100	4.036	4.168
1009665142487836032	0.597	9.814	0.245	0.084	4.148	5.169
1058066262817534336	0.660	9.773	0.332	0.094	3.794	4.047
1286188056265485952	0.377	10.414	0.378	0.122	4.106	5.006
1374971558625266432	0.622	10.939	0.371	0.129	3.759	3.734
1483653713185923072	0.552	10.544	0.284	0.092	3.897	4.471
1533880980593444352	0.698	12.041	0.298	0.099	4.029	4.733
1561928427003019520	0.468	10.761	0.369	0.092	4.207	5.079
1683444631038133248	0.570	10.458	0.312	0.104	4.058	4.873
1760981190300823808	0.473	9.572	0.248	0.077	4.003	5.100
2099623285533405952	0.682	12.243	0.374	0.161	4.173	4.586
2110264427784391168	0.441	10.841	0.407	0.079	4.148	5.213
2142052889490819328	0.467	9.386	0.431	0.108	3.964	4.636
2254366868398077312	0.476	10.064	0.355	0.080	4.072	4.828
2373827054405627904	0.574	11.356	0.268	0.074	3.748	3.984
2381771781829913984	0.634	11.108	0.245	0.088	4.140	5.279
2438710609949867776	0.482	11.425	0.294	0.063	4.511	6.200
2497458508359533184	0.548	12.530	0.310	0.032	4.716	0.334
2558296724402139392	0.553	9.673	0.296	0.108	3.854	4.129
2689556491246048896	0.459	10.984	0.449	0.206	3.935	4.060

2828497068363486720	0.641	10.222	0.214	0.089	3.972	5.172
3626569264033312896	0.553	11.875	0.311	0.091	3.669	3.433
3797319369672686592	0.626	11.060	0.311	0.064	3.911	4.349
4224859720193721856	0.362	11.687	0.432	0.147	4.163	4.957
4593112037219674368	0.577	11.643	0.339	0.106	4.172	5.029
4596935593202765184	0.400	11.225	0.396	0.143	3.878	4.259
4709830423483623808	0.642	11.410	0.370	0.117	3.811	4.041
5510293236607430656	0.391	10.829	0.412	0.153	4.031	4.471
5769986338215537280	0.571	10.503	0.341	0.146	3.927	4.476
5773390391856998656	0.587	11.955	0.359	0.128	3.952	4.550
6380659528686603008	0.550	12.767	0.323	0.091	4.004	4.433
6483680332235888896	0.480	9.878	0.378	0.117	3.913	4.083
6680420204104678272	0.553	11.236	0.305	0.088	4.387	5.474
6771307454464848768	0.477	10.155	0.372	0.077	3.953	4.115
5743059538967112576	0.537	11.253	0.299	0.011	4.077	0.009
6226585956422527616	0.699	12.137	0.303	0.090	3.916	4.819
2052162282013412992	0.487	15.001	0.449	0.113	4.448	5.463
2073301252055048704	0.548	14.817	0.383	0.078	4.319	5.434
2073691475601022336	0.524	14.134	0.239	0.071	3.934	4.826
2073795929206140416	0.621	13.727	0.327	0.121	3.843	4.249
2075326037075060352	0.534	14.889	0.293	0.048	4.765	1.277
2080455705486937728	0.533	15.443	0.362	0.095	4.061	4.772
2101971601853190912	0.684	12.968	0.260	0.067	4.026	4.908
2102990574253407744	0.456	16.382	0.420	0.124	4.003	4.250
2104438871583819904	0.488	13.336	0.237	0.064	4.014	4.818
2104473677999021312	0.562	15.976	0.273	0.056	4.024	5.034
2105004192359662336	0.474	14.127	0.435	0.138	4.092	4.273

2105468529864072704	0.588	13.246	0.320	0.109	4.094	4.805
2106556462259590272	0.558	15.969	0.257	0.054	4.380	5.922
2119119619555858944	0.594	15.692	0.337	0.099	3.836	3.842
2127818405800967936	0.549	13.329	0.210	0.094	3.935	4.506
2127827579851196800	0.434	14.349	0.323	0.107	3.994	4.803
2128131113782390144	0.557	16.572	0.314	0.111	4.129	4.953
2130324914355524992	0.527	16.357	0.339	0.115	4.517	6.166
2131968508140833920	0.613	11.659	0.205	0.050	4.273	5.813
2132161064413068160	0.687	12.712	0.330	0.107	3.867	4.531
2133132895253493760	0.436	14.553	0.440	0.202	3.946	4.296
5412243359495900928	0.574	11.246	0.318	0.089	3.786	4.035
6570585628216929408	0.570	14.090	0.312	0.089	3.847	4.121
6573170751851975936	0.669	14.830	0.250	0.070	4.147	4.588

Table B.1: Table of Fourier coefficients evaluated by the python routine for the stars other than that mentioned in 3.3

C Photometric [Fe/H] table

Gaia ID	**Period**	ϕ_{31}	**[Fe/H]**	**[Fe/H] error**	**[Fe/H] predicted**	**[Fe/H] predicted (error)**
4784552718312266624	0.440	5.494	-0.6	0.13	-0.7027	0.6755
2414817603803476864	0.606	5.499	-1.75	0.13	-1.4745	0.7237
6730211038418525056	0.589	5.599	-1.55	0.13	-1.3098	0.7280
5283957629860435072	0.571	5.345	-1.6	0.13	-1.4414	0.6975
4417888542753226112	0.714	5.323	-1.95	0.13	-2.1318	0.7448
5461994302138361728	0.574	4.959	-1.8	0.13	-1.7914	0.6619

5918501428232052992	0.589	5.649	-1	0.13	-1.2634	0.7326
3587566361077304704	0.733	5.759	-1.7	0.13	-1.8433	0.7912
6787617919184986496	0.587	5.681	-1.65	0.13	-1.2274	0.7353
4825302302864705152	0.487	5.353	-1.55	0.13	-1.0446	0.6736
234108363683247616	0.426	5.197	-0.41	0.1	-0.8899	0.6413
315028326379733760	0.563	5.898	-1.51	0.12	-0.9294	0.7494
630421935431871232	0.452	4.626	-1.49	0.1	-1.5082	0.5914
1009665142487836032	0.597	5.292	-1.64	0.1	-1.6123	0.7011
1058066262817534336	0.660	5.232	-1.91	0.1	-1.9593	0.7170
1286188056265485952	0.377	5.256	-0.49	0.1	-0.6135	0.6357
1374971558625266432	0.622	5.025	-1.77	0.1	-1.9594	0.6845
1483653713185923072	0.552	5.346	-1.32	0.14	-1.3520	0.6918
1533880980593444352	0.698	5.211	-2.35	0.13	-2.1521	0.7287
1561928427003019520	0.468	5.025	-1.39	0.1	-1.2375	0.6354
1683444631038133248	0.570	5.265	-1.33	0.1	-1.5063	0.6895
1760981190300823808	0.473	5.658	-0.54	0.1	-0.7128	0.7004
2099623285533405952	0.682	4.633	-2.68	0.11	-2.5770	0.6714
2110264427784391168	0.441	5.335	-0.44	0.1	-0.8424	0.6594
2142052889490819328	0.467	5.310	-1.7	0.1	-0.9845	0.6636
2254366868398077312	0.476	5.178	-0.96	0.1	-1.1446	0.6531
2373827054405627904	0.574	5.308	-1.52	0.1	-1.4880	0.6949
2381771781829913984	0.634	5.425	-1.9	0.15	-1.6679	0.7257
2438710609949867776	0.482	5.234	-0.83	0.1	-1.1217	0.6602
2558296724402139392	0.553	5.133	-1.55	0.1	-1.5415	0.6716
2689556491246048896	0.459	4.823	-1.52	0.15	-1.3705	0.6129
2828497068363486720	0.641	5.822	-1.59	0.1	-1.3590	0.7659
3626569264033312896	0.553	4.993	-1.82	0.1	-1.6643	0.6583

3797319369672686592	0.626	5.182	-2.05	0.1	-1.8432	0.7004
4224859720193721856	0.362	5.035	-0.46	0.1	-0.7311	0.6092
4593112037219674368	0.577	5.078	-1.49	0.1	-1.7019	0.6741
4596935593202765184	0.400	5.192	-0.49	0.1	-0.7722	0.6344
4709830423483623808	0.642	5.173	-1.9	0.15	-1.9252	0.7052
5510293236607430656	0.391	4.943	-1.07	0.15	-0.9462	0.6065
5769986338215537280	0.571	5.260	-1.64	0.1	-1.5168	0.6896
5773390391856998656	0.587	5.259	-1.92	0.1	-1.5936	0.6946
6380659528686603008	0.550	4.989	-1.79	0.1	-1.6521	0.6568
6483680332235888896	0.480	4.910	-1.6	0.14	-1.3908	0.6273
6680420204104678272	0.553	4.880	-2.07	0.1	-1.7596	0.6474
6771307454464848768	0.477	4.822	-1.29	0.1	-1.4565	0.6181
6226585956422527616	0.699	5.636	-1.61	0.22	-1.7893	0.7677
2052162282013412992	0.487	4.684	-1.8	0.13	-1.6201	0.6075
2073691475601022336	0.524	5.590	-0.56	0.1	-1.0099	0.7075
2073795929206140416	0.621	5.285	-1.3	0.1	-1.7273	0.7082
2080455705486937728	0.533	5.154	-1.42	0.14	-1.4309	0.6674
2101971601853190912	0.684	5.396	-1.47	0.1	-1.9264	0.7403
2102990574253407744	0.456	4.806	-1.42	0.1	-1.3718	0.6104
2104438871583819904	0.488	5.343	-0.3	0.1	-1.0567	0.6729
2104473677999021312	0.562	5.529	-1.58	0.1	-1.2412	0.7126
2105004192359662336	0.474	4.562	-1.28	0.1	-1.6630	0.5915
2105468529864072704	0.588	5.089	-2.03	0.1	-1.7429	0.6787
2106556462259590272	0.558	5.348	-1.64	0.1	-1.3773	0.6938
2119119619555858944	0.594	4.899	-1.97	0.1	-1.9363	0.6631
2127818405800967936	0.549	5.267	-0.73	0.1	-1.4055	0.6831
2127827579851196800	0.434	5.388	-0.19	0.1	-0.7633	0.6630

2128131113782390144	0.557	5.131	-1.41	0.15	-1.5615	0.6726
2130324914355524992	0.527	5.181	-1.3	0.1	-1.3783	0.6682
2131968508140833920	0.613	5.562	-1.23	0.1	-1.4536	0.7320
2132161064413068160	0.687	5.498	-1.47	0.1	-1.8554	0.7510
2133132895253493760	0.436	5.025	-1.37	0.15	-1.0890	0.6267
5412243359495900928	0.574	5.245	-1.92	0.1	-1.5414	0.6888
6570585628216929408	0.570	5.146	-2.13	0.1	-1.6100	0.6783
6573170751851975936	0.669	4.714	-2.89	0.1	-2.4452	0.6734

Table C.1: Table of spectroscopic and photometric metallicities along with their errors for the stars other than that mentioned in Table 4.1

Bibliography

References

1. Boggs, P. T. and Rogers, J. E. (1990). Orthogonal distance regression. *Contemporary mathematics*, 112:183–194.

2. Calzetti, D., Armus, L., Bohlin, R. C., Kinney, A. L., Koornneef, J., and Storchi-Bergmann, T. (2000). The Dust Content and Opacity of Actively Star-forming Galaxies. , 533(2):682–695.

3. Carretta, E., Bragaglia, A., Gratton, R., D'Orazi, V., and Lucatello, S. (2009). Intrinsic iron spread and a new metallicity scale for globular clusters. , 508(2):695–706.

4. Chadid, M., Sneden, C., and Preston, G. W. (2017). Spectroscopic Comparison of Metal-rich RRab Stars of the Galactic Field with their Metal-poor Counterparts. , 835(2):187.

5. Clementini, G., Ripepi, V., Leccia, S., Mowlavi, N., Lecoeur-Taibi, I., Marconi, M., Szabados, L., Eyer, L., Guy, L. P., Rimoldini, L., Jevardat de Fombelle, G., Holl, B., Busso, G., Charnas, J., Cuypers, J., De Angeli, F., De Ridder, J., Debosscher, J., Evans, D. W., Klagyivik, P., Musella, I., Nienartowicz, K., Ordóñez, D., Regibo, S., Riello, M., Sarro, L. M., and Süveges, M. (2016). Gaiadata release 1: The cepheid and rr lyrae star pipeline and its application to the south ecliptic pole region. *Astronomy amp; Astrophysics*, 595:A133.

6. Gaia Collaboration, Vallenari, A., Brown, A. G. A., Prusti, T., de Bruijne, J. H. J., Arenou, F., Babusiaux, C., Biermann, M., Creevey, O. L., Ducourant, C., Evans, D. W., Eyer, L., Guerra, R., Hutton, A., Jordi, C., Klioner, S. A., Lammers, U. L., Lindegren, L., Luri, X., Mignard, F., Panem, C., Pourbaix, D., Randich, S., Sartoretti, P., Soubiran, C., Tanga, P., Walton, N. A., Bailer-Jones, C. A. L., Bastian, U., Drimmel, R., Jansen, F., Katz, D., Lattanzi, M. G., van Leeuwen, F., Bakker, J., Cacciari, C., Castañeda, J., De Angeli, F., Fabricius, C., Fouesneau, M., Frémat, Y., Galluccio, L., Guerrier, A., Heiter, U., Masana, E., Messineo, R., Mowlavi, N., Nicolas, C., Nienartowicz, K., Pailler, F., Panuzzo, P., Riclet, F., Roux, W., Seabroke, G. M., Sordo, R., Thévenin, F., Gracia-Abril, G., Portell, J., Teyssier, D., Altmann, M., Andrae, R., Audard, M., Bellas-Velidis,

I., Benson, K., Berthier, J., Blomme, R., Burgess, P. W., Busonero, D., Busso, G., Cánovas, H., Carry, B., Cellino, A., Cheek, N., Clementini, G., Damerdji, Y., Davidson, M., de Teodoro, P., Nuñez Campos, M., Delchambre, L., Dell'Oro, A., Esquej, P., Fernández-Hernández, J., Fraile, E., Garabato, D., García-Lario, P., Gosset, E., Haigron, R., Halbwachs, J. L., Hambly, N. C., Harrison, D. L., Hernández, J., Hestroffer, D., Hodgkin, S. T., Holl, B., Janßen, K., Jevardat de Fombelle, G., Jordan, S., Krone-Martins, A., Lanzafame, A. C., Löffler, W., Marchal, O., Marrese, P. M., Moitinho, A., Muinonen, K., Osborne, P., Pancino, E., Pauwels, T., Recio-Blanco, A., Reylé, C., Riello, M., Rimoldini, L., Roegiers, T., Rybizki, J., Sarro, L. M., Siopis, C., Smith, M., Sozzetti, A., Utrilla, E., van Leeuwen, M., Abbas, U., Ábrahám, P., Abreu Aramburu, A., Aerts, C., Aguado, J. J., Ajaj, M., Aldea-Montero, F., Altavilla, G., Álvarez, M. A., Alves, J., Anders, F., Anderson, R. I., Anglada Varela, E., Antoja, T., Baines, D., Baker, S. G., Balaguer-Núñez, L., Balbinot, E., Balog, Z., Barache, C., Barbato, D., Barros, M., Barstow, M. A., Bartolomé, S., Bassilana, J. L., Bauchet, N., Becciani, U., Bellazzini, M., Berihuete, A., Bernet, M., Bertone, S., Bianchi, L., Binnenfeld, A., Blanco-Cuaresma, S., Blazere, A., Boch, T., Bombrun, A., Bossini, D., Bouquillon, S., Bragaglia, A., Bramante, L., Breedt, E., Bressan, A., Brouillet, N., Brugaletta, E., Bucciarelli, B., Burlacu, A., Butkevich, A. G., Buzzi, R., Caffau, E., Cancelliere, R., Cantat-Gaudin, T., Carballo, R., Carlucci, T., Carnerero, M. I., Carrasco, J. M., Casamiquela, L., Castellani, M., Castro-Ginard, A., Chaoul, L., Charlot, P., Chemin, L., Chiaramida, V., Chiavassa, A., Chornay, N., Comoretto, G., Contursi, G., Cooper, W. J., Cornez, T., Cowell, S., Crifo, F., Cropper, M., Crosta, M., Crowley, C., Dafonte, C., Dapergolas, A., David, M., David, P., de Laverny, P., De Luise, F., De March, R., De Ridder, J., de Souza, R., de Torres, A., del Peloso, E. F., del Pozo, E., Delbo, M., Delgado, A., Delisle, J. B., Demouchy, C., Dharmawardena, T. E., Di Matteo, P., Diakite, S., Diener, C., Distefano, E., Dolding, C., Edvardsson, B., Enke, H., Fabre, C., Fabrizio, M., Faigler, S., Fedorets, G., Fernique, P., Fienga, A., Figueras, F., Fournier, Y., Fouron, C., Fragkoudi, F., Gai, M., Garcia-Gutierrez, A., Garcia-Reinaldos, M., García-Torres, M., Garofalo, A., Gavel, A., Gavras, P., Gerlach, E., Geyer, R., Giacobbe, P., Gilmore, G., Girona, S., Giuffrida, G., Gomel, R., Gomez, A., González-Núñez, J., González-Santamaría, I., González-Vidal, J. J., Granvik, M., Guillout, P., Guiraud, J., Gutiérrez-Sánchez, R., Guy, L. P., Hatzidimitriou, D., Hauser, M.,

Haywood, M., Helmer, A., Helmi, A., Sarmiento, M. H., Hidalgo, S. L., Hilger, T., Hładczuk, N., Hobbs, D., Holland, G., Huckle, H. E., Jardine, K., Jasniewicz, G., Jean-Antoine Piccolo, A., Jiménez-Arranz, Ó., Jorissen, A., Juaristi Campillo, J., Julbe, F., Karbevska, L., Kervella, P., Khanna, S., Kontizas, M., Kordopatis, G., Korn, A. J., Kóspál, Á., Kostrzewa-Rutkowska, Z., Kruszyńska, K., Kun, M., Laizeau, P., Lambert, S., Lanza, A. F., Lasne, Y., Le Campion, J. F., Lebreton, Y., Lebzelter, T., Leccia, S., Leclerc, N., Lecoeur-Taibi, I., Liao, S., Licata, E. L., Lindstrøm, H. E. P., Lister, T. A., Livanou, E., Lobel, A., Lorca, A., Loup, C., Madrero Pardo, P., Magdaleno Romeo, A., Managau, S., Mann, R. G., Manteiga, M., Marchant, J. M., Marconi, M., Marcos, J., Marcos Santos, M. M. S., Marín Pina, D., Marinoni, S., Marocco, F., Marshall, D. J., Martin Polo, L., Martín-Fleitas, J. M., Marton, G., Mary, N., Masip, A., Massari, D., Mastrobuono-Battisti, A., Mazeh, T., McMillan, P. J., Messina, S., Michalik, D., Millar, N. R., Mints, A., Molina, D., Molinaro, R., Molnár, L., Monari, G., Monguió, M., Montegriffo, P., Montero, A., Mor, R., Mora, A., Morbidelli, R., Morel, T., Morris, D., Muraveva, T., Murphy, C. P., Musella, I., Nagy, Z., Noval, L., Ocaña, F., Ogden, A., Ordenovic, C., Osinde, J. O., Pagani, C., Pagano, I., Palaversa, L., Palicio, P. A., Pallas-Quintela, L., Panahi, A., Payne-Wardenaar, S., Peñalosa Esteller, X., Penttilä, A., Pichon, B., Piersimoni, A. M., Pineau, F. X., Plachy, E., Plum, G., Poggio, E., Prša, A., Pulone, L., Racero, E., Ragaini, S., Rainer, M., Raiteri, C. M., Rambaux, N., Ramos, P., Ramos-Lerate, M., Re Fiorentin, P., Regibo, S., Richards, P. J., Rios Diaz, C., Ripepi, V., Riva, A., Rix, H. W., Rixon, G., Robichon, N., Robin, A. C., Robin, C., Roelens, M., Rogues, H. R. O., Rohrbasser, L., Romero-Gómez, M., Rowell, N., Royer, F., Ruz Mieres, D., Rybicki, K. A., Sadowski, G., Sáez Núñez, A., Sagristà Sellés, A., Sahlmann, J., Salguero, E., Samaras, N., Sanchez Gimenez, V., Sanna, N., Santoveña, R., Sarasso, M., Schultheis, M., Sciacca, E., Segol, M., Segovia, J. C., Ségransan, D., Semeux, D., Shahaf, S., Siddiqui, H. I., Siebert, A., Siltala, L., Silvelo, A., Slezak, E., Slezak, I., Smart, R. L., Snaith, O. N., Solano, E., Solitro, F., Souami, D., Souchay, J., Spagna, A., Spina, L., Spoto, F., Steele, I. A., Steidelmüller, H., Stephenson, C. A., Süveges, M., Surdej, J., Szabados, L., Szegedi-Elek, E., Taris, F., Taylor, M. B., Teixeira, R., Tolomei, L., Tonello, N., Torra, F., Torra, J., Torralba Elipe, G., Trabucchi, M., Tsounis, A. T., Turon, C., Ulla, A., Unger, N., Vaillant, M. V., van Dillen, E., van Reeven, W., Vanel, O., Vecchiato, A., Viala, Y.,

Vicente, D., Voutsinas, S., Weiler, M., Wevers, T., Wyrzykowski, Ł., Yoldas, A., Yvard, P., Zhao, H., Zorec, J., Zucker, S., and Zwitter, T. (2023). Gaia Data Release 3. Summary of the content and survey properties. , 674:A1.

7. Gilligan, C. K., Chaboyer, B., Marengo, M., Mullen, J. P., Bono, G., Braga, V. F., Crestani, J., Dall'Ora, M., Fiorentino, G., Monelli, M., Neeley, J. R., Fabrizio, M., Martínez-Vázquez, C. E., Thévenin, F., and Sneden, C. (2021). Metallicities from high-resolution spectra of 49 RR Lyrae variables. , 503(4):4719–4733.

8. Iorio, G. and Belokurov, V. (2021). Chemo-kinematics of the Gaia RR Lyrae: the halo and the disc. , 502(4):5686–5710.

9. Jurcsik, J. (1995). Revision of the [Fe/H] Scales Used for Globular Clusters and RR Lyrae Variables. , 45:653–660.

10. Jurcsik, J. and Kovacs, G. (1996). Determination of [Fe/H] from the light curves of RR Lyrae stars. , 312:111–120.

11. Kapakos, E., Hatzidimitriou, D., and Soszyński, I. (2011). RR Lyrae variables in the Small Magellanic Cloud – I. The central region. *Monthly Notices of the Royal Astronomical Society*, 415(2):1366–1380.

12. Koch, D. G., Borucki, W. J., Basri, G., Batalha, N. M., Brown, T. M., Caldwell, D., Christensen-Dalsgaard, J., Cochran, W. D., DeVore, E., Dunham, E. W., Gautier, Thomas N., I., Geary, J. C., Gilliland, R. L., Gould, A., Jenkins, J., Kondo, Y., Latham, D. W., Lissauer, J. J., Marcy, G., Monet, D., Sasselov, D., Boss, A., Brownlee, D., Caldwell, J., Dupree, A. K., Howell, S. B., Kjeldsen, H., Meibom, S., Morrison, D., Owen, T., Reitsema, H., Tarter, J., Bryson, S. T., Dotson, J. L., Gazis, P., Haas, M. R., Kolodziejczak, J., Rowe, J. F., Van Cleve, J. E., Allen, C., Chandrasekaran, H., Clarke, B. D., Li, J., Quintana, E. V., Tenenbaum, P., Twicken, J. D., and Wu, H. (2010). Kepler Mission Design, Realized Photometric Performance, and Early Science. , 713(2):L79–L86.

13. Liu, G. C., Huang, Y., Zhang, H. W., Xiang, M. S., Ren, J. J., Chen, B. Q., Yuan, H. B., Wang,

C., Yang, Y., Tian, Z. J., Wang, F., and Liu, X. W. (2020). Probing the Galactic Halo with RR Lyrae Stars. I. The Catalog. , 247(2):68.

14. Martinez-Vazquez, C. E., Monelli, M., Bono, G., Stetson, P. B., Gallart, C., Bernard, E. J., Fiorentino, G., and Dall'Ora, M. (2016). A new Phi_31-period-metallicity relation for RR Lyrae stars. *Commmunications of the Konkoly Observatory Hungary*, 105:53–56.

15. Mullen, J. P., Marengo, M., Martínez-Vázquez, C. E., Neeley, J. R., Bono, G., Dall'Ora, M., Chaboyer, B., Thévenin, F., Braga, V. F., Crestani, J., Fabrizio, M., Fiorentino, G., Gilligan, C. K., Monelli, M., and Stetson, P. B. (2021). Metallicity of Galactic RR Lyrae from Optical and Infrared Light Curves. I. Period-Fourier-Metallicity Relations for Fundamental-mode RR Lyrae. , 912(2):144.

16. Nemec, J. M., Cohen, J. G., Ripepi, V., Derekas, A., Moskalik, P., Sesar, B., Chadid, M., and Bruntt, H. (2013). Metal Abundances, Radial Velocities, and Other Physical Characteristics for the RR Lyrae Stars in The Kepler Field. , 773(2):181.

17. Nemec, J. M., Smolec, R., Benkő, J. M., Moskalik, P., Kolenberg, K., Szabó, R., Kurtz, D. W., Bryson, S., Guggenberger, E., Chadid, M., Jeon, Y. B., Kunder, A., Layden, A. C., Kinemuchi, K., Kiss, L. L., Poretti, E., Christensen-Dalsgaard, J., Kjeldsen, H., Caldwell, D., Ripepi, V., Derekas, A., Nuspl, J., Mullally, F., Thompson, S. E., and Borucki, W. J. (2011). Fourier analysis of non-Blazhko ab-type RR Lyrae stars observed with the Kepler space telescope. , 417(2):1022–1053.

18. Ngeow, C.-C., Yu, P.-C., Bellm, E., Yang, T.-C., Chang, C.-K., Miller, A., Laher, R., Surace, J., and Ip, W.-H. (2016). The Palomar Transient Factory and RR Lyrae: The Metallicity-Light Curve Relation Based on ab-type RR Lyrae in the Kepler Field. , 227(2):30.

19. Prusti, T., de Bruijne, J. H. J., Brown, A. G. A., Vallenari, A., Babusiaux, C., Bailer-Jones, C. A. L., Bastian, U., Biermann, M., Evans, D. W., Eyer, L., Jansen, F., Jordi, C., Klioner, S. A., Lammers, U., Lindegren, L., Luri, X., Mignard, F., Milligan, D. J., Panem, C., Poinsignon, V., Pourbaix, D., Randich, S., Sarri, G., Sartoretti, P., Siddiqui, H. I., Soubiran, C., Valette, V., van Leeuwen, F., Walton, N. A., Aerts, C., Arenou, F., Cropper, M., Drimmel, R., Høg, E., Katz, D., Lattanzi, M. G., O'Mullane, W., Grebel, E. K., Holland, A. D., Huc, C., Passot, X., Bramante,

L., Cacciari, C., Castañeda, J., Chaoul, L., Cheek, N., De Angeli, F., Fabricius, C., Guerra, R., Hernández, J., Jean-Antoine-Piccolo, A., Masana, E., Messineo, R., Mowlavi, N., Nienartowicz, K., Ordóñez-Blanco, D., Panuzzo, P., Portell, J., Richards, P. J., Riello, M., Seabroke, G. M., Tanga, P., Thévenin, F., Torra, J., Els, S. G., Gracia-Abril, G., Comoretto, G., Garcia-Reinaldos, M., Lock, T., Mercier, E., Altmann, M., Andrae, R., Astraatmadja, T. L., Bellas-Velidis, I., Benson, K., Berthier, J., Blomme, R., Busso, G., Carry, B., Cellino, A., Clementini, G., Cowell, S., Creevey, O., Cuypers, J., Davidson, M., De Ridder, J., de Torres, A., Delchambre, L., Dell'Oro, A., Ducourant, C., Frémat, Y., García-Torres, M., Gosset, E., Halbwachs, J.-L., Hambly, N. C., Harrison, D. L., Hauser, M., Hestroffer, D., Hodgkin, S. T., Huckle, H. E., Hutton, A., Jasniewicz, G., Jordan, S., Kontizas, M., Korn, A. J., Lanzafame, A. C., Manteiga, M., Moitinho, A., Muinonen, K., Osinde, J., Pancino, E., Pauwels, T., Petit, J.-M., Recio-Blanco, A., Robin, A. C., Sarro, L. M., Siopis, C., Smith, M., Smith, K. W., Sozzetti, A., Thuillot, W., van Reeven, W., Viala, Y., Abbas, U., Abreu Aramburu, A., Accart, S., Aguado, J. J., Allan, P. M., Allasia, W., Altavilla, G., Álvarez, M. A., Alves, J., Anderson, R. I., Andrei, A. H., Anglada Varela, E., Antiche, E., Antoja, T., Antón, S., Arcay, B., Atzei, A., Ayache, L., Bach, N., Baker, S. G., Balaguer-Núñez, L., Barache, C., Barata, C., Barbier, A., Barblan, F., Baroni, M., Barrado y Navascués, D., Barros, M., Barstow, M. A., Becciani, U., Bellazzini, M., Bellei, G., Bello García, A., Belokurov, V., Bendjoya, P., Berihuete, A., Bianchi, L., Bienaymé, O., Billebaud, F., Blagorodnova, N., Blanco-Cuaresma, S., Boch, T., Bombrun, A., Borrachero, R., Bouquillon, S., Bourda, G., Bouy, H., Bragaglia, A., Breddels, M. A., Brouillet, N., Brüsemeister, T., Bucciarelli, B., Budnik, F., Burgess, P., Burgon, R., Burlacu, A., Busonero, D., Buzzi, R., Caffau, E., Cambras, J., Campbell, H., Cancelliere, R., Cantat-Gaudin, T., Carlucci, T., Carrasco, J. M., Castellani, M., Charlot, P., Charnas, J., Charvet, P., Chassat, F., Chiavassa, A., Clotet, M., Cocozza, G., Collins, R. S., Collins, P., Costigan, G., Crifo, F., Cross, N. J. G., Crosta, M., Crowley, C., Dafonte, C., Damerdji, Y., Dapergolas, A., David, P., David, M., De Cat, P., de Felice, F., de Laverny, P., De Luise, F., De March, R., de Martino, D., de Souza, R., Debosscher, J., del Pozo, E., Delbo, M., Delgado, A., Delgado, H. E., di Marco, F., Di Matteo, P., Diakite, S., Distefano, E., Dolding, C., Dos Anjos, S., Drazinos, P., Durán, J., Dzigan, Y., Ecale, E., Edvardsson, B., Enke, H., Erdmann, M., Escolar, D., Espina, M., Evans, N. W., Eynard Bontemps,

G., Fabre, C., Fabrizio, M., Faigler, S., Falcão, A. J., Farràs Casas, M., Faye, F., Federici, L., Fedorets, G., Fernández-Hernández, J., Fernique, P., Fienga, A., Figueras, F., Filippi, F., Findeisen, K., Fonti, A., Fouesneau, M., Fraile, E., Fraser, M., Fuchs, J., Furnell, R., Gai, M., Galleti, S., Galluccio, L., Garabato, D., García-Sedano, F., Garé, P., Garofalo, A., Garralda, N., Gavras, P., Gerssen, J., Geyer, R., Gilmore, G., Girona, S., Giuffrida, G., Gomes, M., González-Marcos, A., González-Núñez, J., González-Vidal, J. J., Granvik, M., Guerrier, A., Guillout, P., Guiraud, J., Gúrpide, A., Gutiérrez-Sánchez, R., Guy, L. P., Haigron, R., Hatzidimitriou, D., Haywood, M., Heiter, U., Helmi, A., Hobbs, D., Hofmann, W., Holl, B., Holland, G., Hunt, J. A. S., Hypki, A., Icardi, V., Irwin, M., Jevardat de Fombelle, G., Jofré, P., Jonker, P. G., Jorissen, A., Julbe, F., Karampelas, A., Kochoska, A., Kohley, R., Kolenberg, K., Kontizas, E., Koposov, S. E., Kordopatis, G., Koubsky, P., Kowalczyk, A., Krone-Martins, A., Kudryashova, M., Kull, I., Bachchan, R. K., Lacoste-Seris, F., Lanza, A. F., Lavigne, J.-B., Le Poncin-Lafitte, C., Lebreton, Y., Lebzelter, T., Leccia, S., Leclerc, N., Lecoeur-Taibi, I., Lemaitre, V., Lenhardt, H., Leroux, F., Liao, S., Licata, E., Lindstrøm, H. E. P., Lister, T. A., Livanou, E., Lobel, A., Löffler, W., López, M., Lopez-Lozano, A., Lorenz, D., Loureiro, T., MacDonald, I., Magalhães Fernandes, T., Managau, S., Mann, R. G., Mantelet, G., Marchal, O., Marchant, J. M., Marconi, M., Marie, J., Marinoni, S., Marrese, P. M., Marschalkó, G., Marshall, D. J., Martín-Fleitas, J. M., Martino, M., Mary, N., Matijevič, G., Mazeh, T., McMillan, P. J., Messina, S., Mestre, A., Michalik, D., Millar, N. R., Miranda, B. M. H., Molina, D., Molinaro, R., Molinaro, M., Molnár, L., Moniez, M., Montegriffo, P., Monteiro, D., Mor, R., Mora, A., Morbidelli, R., Morel, T., Morgenthaler, S., Morley, T., Morris, D., Mulone, A. F., Muraveva, T., Musella, I., Narbonne, J., Nelemans, G., Nicastro, L., Noval, L., Ordénovic, C., Ordieres-Meré, J., Osborne, P., Pagani, C., Pagano, I., Pailler, F., Palacin, H., Palaversa, L., Parsons, P., Paulsen, T., Pecoraro, M., Pedrosa, R., Pentikäinen, H., Pereira, J., Pichon, B., Piersimoni, A. M., Pineau, F.-X., Plachy, E., Plum, G., Poujoulet, E., Prša, A., Pulone, L., Ragaini, S., Rago, S., Rambaux, N., Ramos-Lerate, M., Ranalli, P., Rauw, G., Read, A., Regibo, S., Renk, F., Reylé, C., Ribeiro, R. A., Rimoldini, L., Ripepi, V., Riva, A., Rixon, G., Roelens, M., Romero-Gómez, M., Rowell, N., Royer, F., Rudolph, A., Ruiz-Dern, L., Sadowski, G., Sagristà Sellés, T., Sahlmann, J., Salgado, J., Salguero, E., Sarasso, M., Savietto,

H., Schnorhk, A., Schultheis, M., Sciacca, E., Segol, M., Segovia, J. C., Segransan, D., Serpell, E., Shih, I.-C., Smareglia, R., Smart, R. L., Smith, C., Solano, E., Solitro, F., Sordo, R., Soria Nieto, S., Souchay, J., Spagna, A., Spoto, F., Stampa, U., Steele, I. A., Steidelmüller, H., Stephenson, C. A., Stoev, H., Suess, F. F., Süveges, M., Surdej, J., Szabados, L., Szegedi-Elek, E., Tapiador, D., Taris, F., Tauran, G., Taylor, M. B., Teixeira, R., Terrett, D., Tingley, B., Trager, S. C., Turon, C., Ulla, A., Utrilla, E., Valentini, G., van Elteren, A., Van Hemelryck, E., van Leeuwen, M., Varadi, M., Vecchiato, A., Veljanoski, J., Via, T., Vicente, D., Vogt, S., Voss, H., Votruba, V., Voutsinas, S., Walmsley, G., Weiler, M., Weingrill, K., Werner, D., Wevers, T., Whitehead, G., Wyrzykowski, , Yoldas, A., Žerjal, M., Zucker, S., Zurbach, C., Zwitter, T., Alecu, A., Allen, M., Allende Prieto, C., Amorim, A., Anglada-Escudé, G., Arsenijevic, V., Azaz, S., Balm, P., Beck, M., Bernstein, H.-H., Bigot, L., Bijaoui, A., Blasco, C., Bonfigli, M., Bono, G., Boudreault, S., Bressan, A., Brown, S., Brunet, P.-M., Bunclark, P., Buonanno, R., Butkevich, A. G., Carret, C., Carrion, C., Chemin, L., Chéreau, F., Corcione, L., Darmigny, E., de Boer, K. S., de Teodoro, P., de Zeeuw, P. T., Delle Luche, C., Domingues, C. D., Dubath, P., Fodor, F., Frézouls, B., Fries, A., Fustes, D., Fyfe, D., Gallardo, E., Gallegos, J., Gardiol, D., Gebran, M., Gomboc, A., Gómez, A., Grux, E., Gueguen, A., Heyrovsky, A., Hoar, J., Iannicola, G., Isasi Parache, Y., Janotto, A.-M., Joliet, E., Jonckheere, A., Keil, R., Kim, D.-W., Klagyivik, P., Klar, J., Knude, J., Kochukhov, O., Kolka, I., Kos, J., Kutka, A., Lainey, V., LeBouquin, D., Liu, C., Loreggia, D., Makarov, V. V., Marseille, M. G., Martayan, C., Martinez-Rubi, O., Massart, B., Meynadier, F., Mignot, S., Munari, U., Nguyen, A.-T., Nordlander, T., Ocvirk, P., O'Flaherty, K. S., Olias Sanz, A., Ortiz, P., Osorio, J., Oszkiewicz, D., Ouzounis, A., Palmer, M., Park, P., Pasquato, E., Peltzer, C., Peralta, J., Péturaud, F., Pieniluoma, T., Pigozzi, E., Poels, J., Prat, G., Prod'homme, T., Raison, F., Rebordao, J. M., Risquez, D., Rocca-Volmerange, B., Rosen, S., Ruiz-Fuertes, M. I., Russo, F., Sembay, S., Serraller Vizcaino, I., Short, A., Siebert, A., Silva, H., Sinachopoulos, D., Slezak, E., Soffel, M., Sosnowska, D., Straižys, V., ter Linden, M., Terrell, D., Theil, S., Tiede, C., Troisi, L., Tsalmantza, P., Tur, D., Vaccari, M., Vachier, F., Valles, P., Van Hamme, W., Veltz, L., Virtanen, J., Wallut, J.-M., Wichmann, R., Wilkinson, M. I., Ziaeepour, H., and Zschocke, S. (2016). Thegaiamission. *Astronomy amp; Astrophysics*, 595:A1.

20. Schlafly, E. F. and Finkbeiner, D. P. (2011). Measuring Reddening with Sloan Digital Sky Survey Stellar Spectra and Recalibrating SFD. , 737(2):103.

21. Simon, N. R. and Lee, A. S. (1981). The structural properties of cepheid light curves. , 248:291–297.

22. Smolec, R. (2005). Metallicity dependence of the blazhko effect. *Acta Astronomica*, 55.

23. Zinn, R. and West, M. J. (1984). The globular cluster system of the Galaxy. III. Measurements of radial velocity and metallicity for 60 clusters and a compilation of metallicities for 121 clusters. , 55:45–66.